Morphological Behavior of Thin Linear Low-Density Polyethylene Films

Keesu Jeon and Ramanan Krishnamoorti*

Department of Chemical and Biomolecular Engineering, University of Houston, Houston, Texas 77204-4004

Received March 24, 2008; Revised Manuscript Received July 15, 2008

ABSTRACT: The crystalline morphology in thin and ultrathin films of linear low-density polyethylene is reported here. Films with thickness ranging from 20 to 800 nm were isothermally crystallized at temperatures ranging from 90 to 119 °C, and the supermolecular and lamellar morphologies were observed by contact and tapping mode atomic force microscopies. Four distinct supermolecular morphologies were observed: banded spherulite, sheaflike, and two intermediate morphologies. The morphological transitions were significant in the films thinner than 200 nm. The sheaflike morphology occurred in the thinner films (<200 nm) while the banded spherulite morphology occurred in the thicker films. The change of morphology was primarily attributed to the change in the extent of lamellar branching. With increased branching, more edge-on lamellae were observed and resulted in changes in the morphology of the thin films. The morphological transitions are discussed on the basis of the chain structure and the unique physical properties of the thin and ultrathin films.

Introduction

Crystallization of polymers is strongly affected by confinement in thin (less than 1000 nm) and ultrathin (less than 100 nm) films. The most significant effects of the confinement are manifested in morphology, crystallinity, kinetics, and melting temperatures,[1] and these have a significant impact on the preparation and use of crystalline polymer based nanocomposite materials.[2] Despotopoulou et al. observed decreases in crystallinity and crystallization rate with decreasing film thickness in thin poly(di-*n*-hexylsilane) (PD6S) films.[1] A critical film thickness (∼15 nm) below which crystallization did not take place was identified for the PD6S films and was reconciled on the basis that this critical film thickness was related to a critical crystal size. On the other hand, poly(ethylene oxide) (PEO) films thinner than 300 nm cast on oxidized silicon wafers showed preferred "flat-on" lamellar crystals.[3,4] The films exhibited decreasing growth rate and crystallinity with decreasing film thickness. The changes in the crystallization behavior of the PEO films were attributed to the decreased mobility of the PEO as a result of attractive interactions between the PEO chains and an oxide layer on the silicon substrate. The reduced growth rate with film thickness was also observed in thin isotactic polystyrene (iPS) films.[5]

Polyolefins and especially polyethylene (PE) represent a class of materials that are relatively simple in terms of interactions with surfaces and further represent a broad range of materials used in coatings and as thin films. The crystallization behavior of PE in thin and ultrathin films is, therefore, quite important commercially and given the simplicity of the interactions and the vast knowledge of their bulk crystalline behavior a fundamental model system to systematically examine the effect of confinement on polymer crystallization. Studies on the crystallization behavior of thin PE films have been carried out recently.[6−10] Mellbring et al.[6] and Bartczak et al.[7] studied the crystallization of high-density polyethylene (HDPE) thin films coated on different substrates. Mellbring et al.[6] observed a shift from a morphology comprising aggregates of edge-on lamellae to a flattened spherulite structure that was observed at a thickness of 100 nm in as-cast spin-coated HDPE films on silicon wafers. A similar morphological shift from the sheaflike morphology (with largely edge-on lamellae) to the banded spherulite morphology was observed in the *nonisothermally* crystallized HDPE films of thickness around 300 nm on calcite surface by Bartczak et al.[7] The preferential growth of edge-on lamellae in the thinner films was explained by the higher rate of secondary nucleation for the crystals in contact with the substrates. Wang et al. investigated the morphology and the melting points in linear low-density polyethylene (LLDPE) thin films coated on HF passivated silicon wafers.[8,9] They observed a banded spherulite structure in the 250 nm film and a sheaflike morphology in the thinner films prepared under *nonisothermal* crystallization conditions. They also observed a significant decrease in the melting temperature for films with thickness below 150 nm. It was argued that the decrease in the melting temperature was caused by a decrease in the equilibrium melting temperature resulting from the attractive interaction between polyethylene chains and the etched silicon substrate. However, at this time it is not clear as to the molecular origins for such an attractive interaction.

Previous studies, as described above, have demonstrated transitions in supermolecular morphology and lamellar structure with changes in film thickness in thin and ultrathin PE films. Those observations provide a preliminary understanding of the consequences of confinement and of chain−substrate interactions on the supermolecular morphology in thin PE films. However, most of those studies were performed with nonisothermally crystallized or as-cast thin films. Therefore, two factors related to the crystalline morphologies, film thickness and consequently the confinement effect, and thermal history could not be separated to understand the morphological transitions. In this study, we focus on the individual effects of confinement and thermal history on the variation of supermolecular and lamellar morphology by performing isothermal studies of crystallization as functions of crystallization temperature and film thickness. Specifically, the confinement induced mass transport limitation to the growing crystal and the role of thermal mobility along with thermodynamic driving force for crystallization are systematically varied in this study. For the purpose, thin and ultrathin LLDPE films with thickness ranging from 20 to 800 nm were fabricated on etched silicon wafers by the spin-coating method, and the films were isothermally crystallized after melting. The supermolecular and lamellar morphologies

* To whom correspondence should be addressed.

10.1021/ma800652p CCC: $40.75
Published on Web 09/13/2008

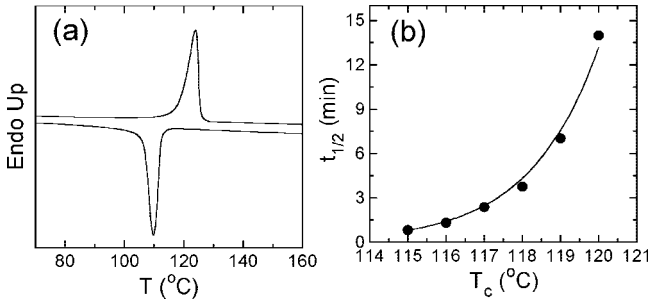

Figure 1. (a) DSC cooling and subsequent heating thermograms at 10 °C/min. (b) Crystallization half-time ($t_{1/2}$) as a function of crystallization temperature (T_c) obtained from isothermal DSC measurements.

were investigated by atomic force microscopy (AFM) in both contact and tapping modes, respectively.

Experimental Section

Materials and Sample Preparation. Linear low-density polyethylene (LLDPE; Union Carbide Co.) was used in this study with a density of 0.918 g/cm^3, a weight-average molecular weight M_w = 410K, and polydispersity M_w/M_n = 5.2. The polymer (~3 g) was dissolved in ~200 mL of boiling toluene, and the solution then poured slowly into ~1 L of methanol at room temperature in order to precipitate the polymer. The precipitated LLDPE was filtered using Whatman qualitative filter papers (Grade 1, 90 mm diameter) and extensively dried at 110 °C overnight in a vacuum oven.

The crystallization and melting peak temperatures, T_{cp} and T_{mp}, respectively, for the LLDPE (~7 mg) were measured using a Perkin-Elmer Pyris 1 differential scanning calorimeter (DSC) and the thermograms (at 10 °C/min) presented in Figure 1a. The values of T_{cp} and T_{mp} are noted to be 109.7 and 124.4 °C, respectively. Temperature and heat flow were calibrated using indium and zinc standards. Isothermal DSC measurements of the LLDPE were also carried out. The LLDPE sample was heated to 160 °C, held at the temperature for 5 min, and cooled at 100 °C/min to a crystallization temperature (T_c) that ranged from 115 to 120 °C. Crystallization half-times ($t_{1/2}$) estimated from the exotherms are shown in Figure 1b.

P-type Si(100) wafers (100 mm diameter, 500−550 μm thick; Silicon Inc.) were used as ~20 × 20 mm^2 pieces. The wafer was cleaned by dipping in a "piranha solution" (a mixture of 30% H_2O_2 and H_2SO_4 (1:2 v/v)) for 10 min and rinsed with running deionized (DI) water for 2 min. The wafer was subsequently dipped in a mixture of 48% HF and DI water (1:50 v/v) for 1 min in order to remove the oxide layer to render the surface hydrophobic[11] and rinsed with running DI water for 30 s. *Caution is required in handling these mixtures. They are corrosive.* Contact angles of DI water on the silicon substrates prior to and after etching by dilute HF solution were measured using a contact angle measuring system G10 (Krüss USA). The angles prior to and after the etching procedure were 0° (completely wetting) and 67 ± 1.2°, respectively, indicating the hydrophobicity of the etched surface.

The cleaned LLDPE was mixed with boiling decalin (~200 °C) for ~1 h on a hot plate using magnetic stirring. The solution was cooled to ~160 °C and maintained at this temperature in a convection oven until spin-coating. A film was prepared by covering a cleaned wafer (preheated to 160−170 °C) with the hot decalin solution of PE and then spinning it at 1800 rpm for 1 min using a spin-coater (Specialty Coating Systems). Pipettes were preheated to 160−170 °C, and the spinner chuck was also preheated to 100−140 °C to prevent the crystallization prior to the spinning process. A smooth surface required few nuclei and depleted spherulite boundaries and was largely controlled by the process of spinning the thin film. The quality of the films strongly depended on the time period over which the wafer along with the chuck accelerated from rest to the spin rate of 1800 rpm. We could obtain

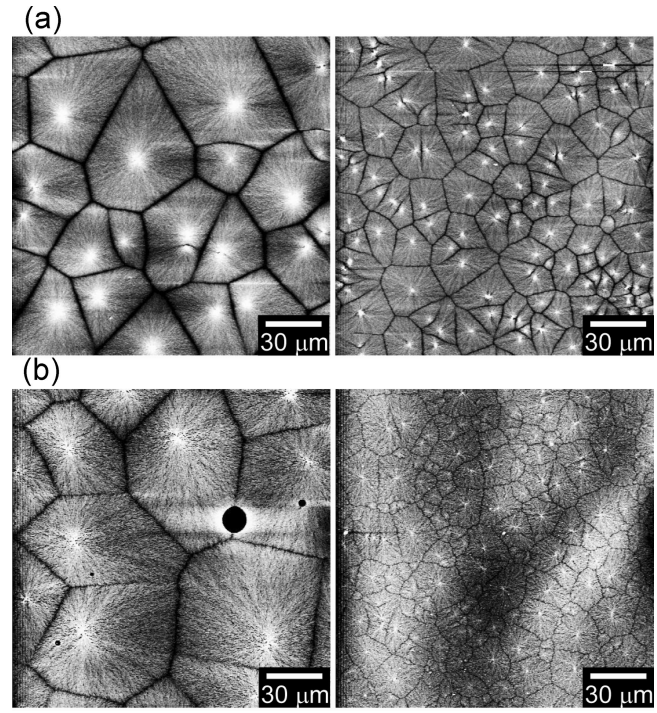

Figure 2. (a) Contact mode AFM images with scan size of 170 μm of the 126 nm thick films spin-coated with an acceleration time of 0.7 s (left) and 0.5 s (right). The films prepared with 0.7 s acceleration time show fewer nuclei and spherulite boundaries. (b) Contact mode AFM images with scan size of 170 μm of ~25 nm thick films spin-coated with (left) or without (right) excess decalin vapor. The number of spherulites are significantly smaller with excess decalin vapor due to the suppressed solvent evaporation, resulting in the reduced crystallization rate during spin-coating.

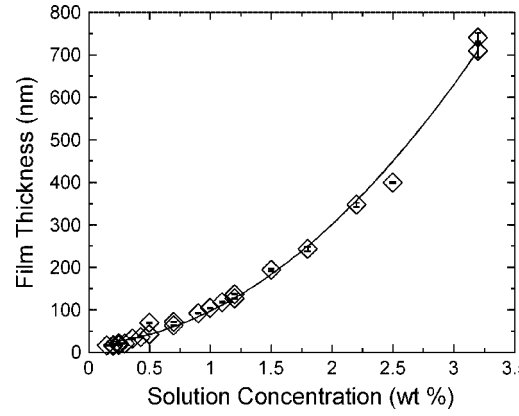

Figure 3. Film thickness of the spin-coated LLDPE films on etched silicon wafers as a function of solution concentration with conditions as described in the text. The line shown represents a best fit polynomial and does not possess any physical significance.

the films with smooth surfaces using an acceleration time of 0.7 s. With shorter acceleration times, more spherulites formed as shown in the right image of Figure 2a, and with longer acceleration times than 0.7 s, the films were not macroscopically uniform. The solvent evaporation rates were also suppressed by ensuring a decalin-rich atmosphere in the spin-coater and therefore to somewhat slower nucleation rates. As presented in Figure 2b, the film (~25 nm thick) exhibits fewer nuclei with excess decalin vapor (the left image), contrasted with more nuclei in the film coated without extra decalin vapor but with otherwise identical conditions.

Thicknesses of as-cast films were measured using an L117 ellipsometer (Gaertner Scientific Co.), and each reported thickness was an average of values obtained at five different spots on each film. The thicknesses of films thicker than 400 nm were additionally

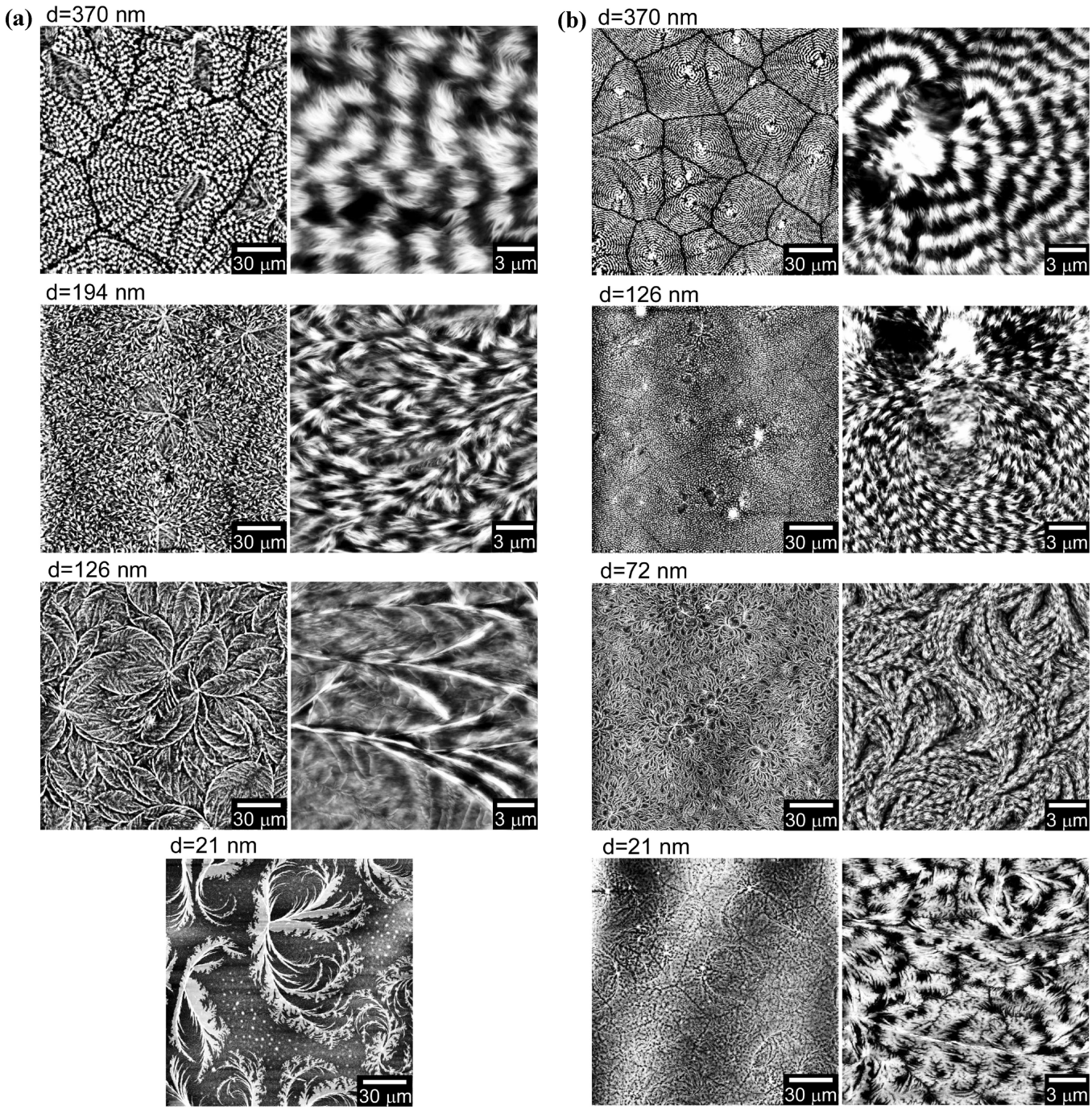

Figure 4. Film thickness dependence of supermolecular morphology by contact mode AFM images with scan sizes of 170 μm (left) and 20 μm (right) of the LLDPE films crystallized at (a) 115 and (b) 90 °C. The 21 nm thick films were held for more than 2 h: 24 h at 115 °C and 10 h at 90 °C to be fully crystallized.

confirmed using a profilometer, Tencor Alpha Step 250 (KLA-Tencor Co.), and those measurements were performed at three different positions on each thin film sample. Several factors control the thickness of spin-coated LLDPE films: concentration of polymer solution, rotational speed, and deposition temperature.[6] In this study, solution concentration, ranging from 0.15 to 3.5 wt %, was used to obtain the desired film thickness at a fixed rotation speed of 1800 rpm and acceleration time of 0.7 s. The film thickness as a function of solution concentration is presented in Figure 3 with the curve of the best fit $d = 62.6c^2 + 15.7c + 18.6$, where d is the film thickness in nm and c the solution concentration in wt %.

For isothermal crystallization studies, a set of spin-coated films were placed in a glass Petri dish (100×15 mm^2) wrapped with an aluminum foil and the films melted at 160 °C for ~2 h in a vacuum oven to erase all prior history in the samples. The wafers (in the Petri dish) were then quickly moved to a second preheated vacuum oven where the films were isothermally crystallized over a temperature range of 90−119 °C for, in most cases, 2 h. Following the isothermal crystallization the films were quickly quenched in liquid nitrogen. In order to verify the robustness of the morphologies reported here, in addition to multiple wafers with identical thickness and thermal histories, we also examined the effect of repeated melting and recrystallization on the supermolecular and lamellar structure. After repeated annealing of the thin films, identical morphologies were observed at each annealing temperature. We note that we did not observe any systematic dewetting of the LLDPE thin films, even for the thinnest samples studied. The rarely observed dewet spots such as those seen in Figure 2b are most likely due to impurities such as dust.

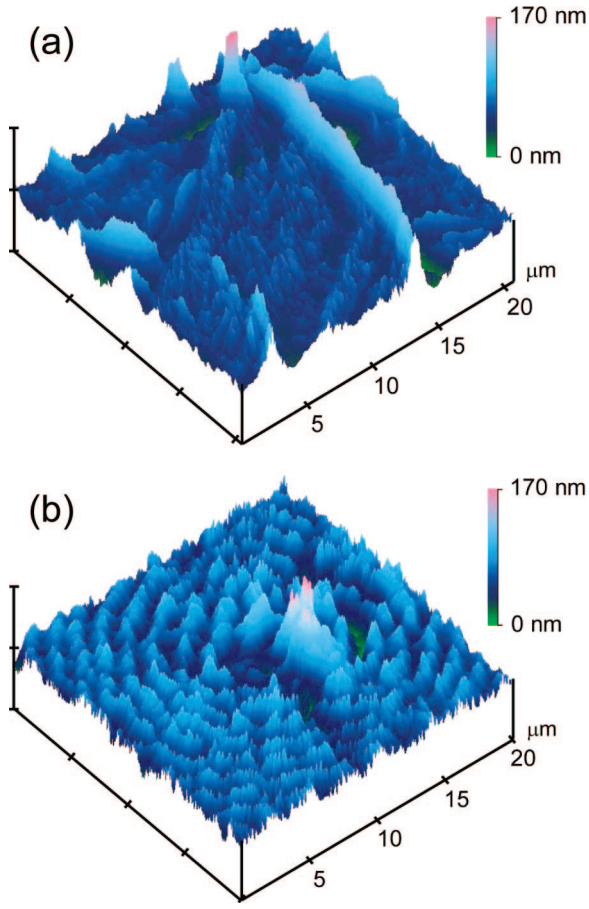

Figure 5. 3D contact mode AFM images for (a) the 126 nm film at 115 °C and (b) the 370 nm film at 90 °C. The sheaflike and banded spherulite morphologies are more clearly demonstrated in these images. The topographically elevated region is observed near the nucleus in each film. In the 126 nm thick film, the sheaflike lamellar bundles are higher than the other regions and keep growing with slight undulation in height along the growing direction. In the 370 nm thick film, the higher regions in banded structure are striped, indicating that the regions are composed of edge-on lamellae.

Atomic Force Microscopy. A scanning probe microscope (SPM), MultiMode Nanoscope E (Digital Instruments), equipped with a J-scanner was employed for contact mode AFM to examine supermolecular morphologies. Contact mode AFM images were obtained at scan rates ranging from 1 to 3 Hz using cantilevers of silicon nitride probes (Veeco Instruments) with a cantilever length of 196 μm, a resonant frequency of ~20 kHz, and a spring constant of 0.12 N/m. Lamellar morphology was examined using tapping mode AFM. Another SPM, MultiMode Nanoscope IIIa (Digital Instruments), with a J-scanner. Tapping mode AFM images were measured at a scan rate of 0.5 Hz, using etched silicon probes (Veeco Instruments) with a cantilever length of 125 μm, a resonant frequency of ~300 kHz, and a spring constant of ~40 N/m. The set point amplitude ratios of the amplitude set point to the free oscillation amplitude were set as ~0.6 (moderate tapping) to properly reflect local stiffness variations on the films.[12] Height and phase images were simultaneously collected. All contact and tapping mode AFM images were taken under ambient conditions at a resolution of 512 × 512 pixels/line. A 450× optical microscope (OM) in the SPM for contact mode AFM was used to count numbers of crystal nuclei in the films. The size of film area monitored by the OM was 490 × 360 μm^2.

Results and Discussion

The supermolecular morphology of isothermally crystallized thin LLDPE films supported on the etched silicon substrates was investigated as a function of film thickness and isothermal crystallization temperature. The morphological studies were primarily conducted using contact mode AFM on samples crystallized ex-situ in a temperature controlled vacuum chamber after melting at an elevated temperature (160 °C) for 2 h. The conditions for melting were confirmed by ensuring that the sample morphology obtained during the spin-casting conditions was completely erased. Contact mode AFM examines the surface topography and is particularly powerful because of the formation of edge-on lamellae and the chain transportation to form the crystalline lamellae, resulting in material depletion and hence thinning of the amorphous or noncrystalline regions.

The effect of film thickness on the crystalline morphology of the LLDPE films supported on the silicon surface is first presented. Two temperatures are chosen as representative sections to elucidate the observed morphologies: one high (115 °C) in reasonable proximity to the bulk melting point and a second low (90 °C), i.e., at large quench depths from the melting temperature. The time for isothermal crystallization in all cases is 2 h with the exception of the 21 nm film, where substantially longer crystallization times were employed. It is noted that the time to obtain fully crystallized films increased with decreasing film thickness, presumably due to a slowing down of the kinetics of crystallization in the ultrathin films.[4,5] The film thickness dependence for the crystalline morphology examined by contact mode AFM at these two temperatures is presented in parts a (115 °C) and b (90 °C) of Figure 4.

The samples crystallized at both temperatures exhibit banded spherulitic structures for the thicker samples and sheaflike morphology for the thinner (sub-150 nm) films. The banded spherulite structure is consistent with the morphology observed in micron-thick films of PE[13,14] and has been attributed to the twisting of lamellae[13,15] or periodic lamellar branching.[16] The banded structure is most clearly seen in the 370 nm films at both temperatures. On the other hand, for the samples crystallized at 115 °C (Figure 4a), the 126 nm and thinner films show the development of sheaflike morphology, and the intermediate thickness samples such as the 194 nm film exhibit a somewhat mixed morphology between the banded spherulites and the sheaflike structures. The sheaflike morphology is quite similar to the morphology observed in the nonisothermally crystallized LLDPE films.[8] Compared with the sheaflike morphology observed in bulk isotactic polystyrene[17] and nylon-6[18] and in thin HDPE films,[6,7] the sheaflike morphology in these LLDPE films studied here shows more open structure in large scales and less sheaflike lamellar aggregates. For the films at 90 °C (Figure 4b), the banded spherulite structure persists down to the 126 nm film, and the sheaflike morphology is observed only in the 21 nm film. The intermediate thickness films as in the 72 nm film also exhibit a mixed morphology between the banded spherulites and the sheaflike structures. We further note that the boundaries observed in the 21 nm thick films do not correspond to the spherulite size as we have observed long lamellae that extend beyond this boundary (Supporting Information, Figure S2b). Such boundaries appear to form during rapid quenching of melt-annealed samples in a liquid nitrogen bath and perhaps represent some overall film instability.

Three-dimensional (3D) images of the topographical features for the 126 nm thick film at 115 °C and the 370 nm thick film at 90 °C, clearly showing the sheaflike morphology and the banded structure, respectively, are presented in Figure 5. In these films the topographically highest regions seem to always occur near the nuclei, which results from the lamellae growing out of free surface among the nucleated lamellae. In the sheaflike morphology (126 nm at 115 °C, Figure 5a), edge-on lamellar bundles are topographically elevated compared to the other regions. The bundles keep growing with slight undulation in

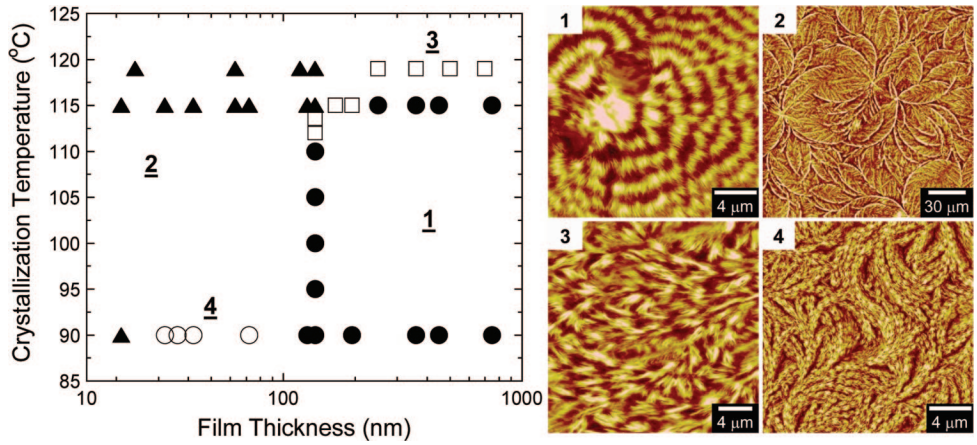

Figure 6. Morphology diagram of the LLDPE thin films. Morphology changes with film thickness and crystallization temperature are monitored and recorded: banded spherulite morphology (1, ●), sheaflike morphology (2, ▲), and intermediate morphologies 3 (□) and 4 (○). The topographic images, shown on the right, represent the different morphologies shown in Figure 6.

Table 1. Categorization of the Morphologies Observed in the Thin LLDPE Films with More General Criteria

criterion	banded	sheaflike	intermediate 3	intermediate 4
rotation symmetry	C_∞	C_2	non	non
continuity	no	yes	no	yes

height along the lamellar growing direction and the regions beside the bundles show a mixed morphology with tilted lamellae and flat-on lamellae. In contrast, the 370 nm film (Figure 5b) shows the banded structure with surface undulation. The higher regions of the band structure are striped, indicating that the regions are composed of edge-on lamellae.

The morphological assignments and transitions are summarized in the morphology diagram presented in Figure 6. In addition to the two well-established (banded spherulite and sheaflike) morphologies, two additional types of intermediate morphologies (3 and 4) are identified between the two established morphologies. In morphology 3, the extent and frequency of lamellar branching are insufficient for the development of a complete banded structure. However, the lamellae are significantly more branched and the surface topography is more undulated than in the sheaflike morphology identified in the thinnest films. As will be observed later in this paper, the banded spherulite morphology possesses edge-on lamellae that lead to striped structures, arranged close to each other and quite different than that observed in morphology 3. Morphology 4 also exhibits

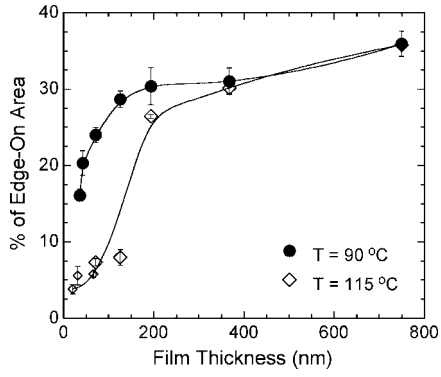

Figure 7. Ratio of area of edge-on lamellar region to total area for the films isothermally crystallized at 90 and 115 °C typically for 2 h. The ratio decreases with film thickness. The decrease is significant in the morphological transitions from the banded spherulite structure to the intermediate morphologies at 90 °C and to the sheaflike morphology at 115 °C. The small diamonds correspond to the films crystallized at 115 °C for 10 h.

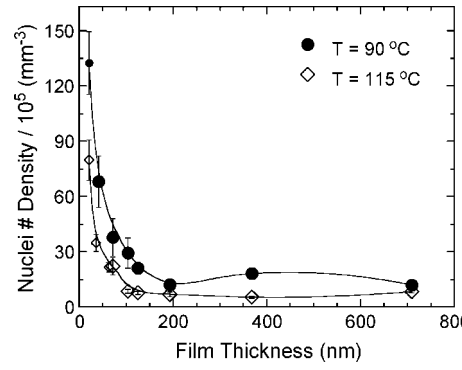

Figure 8. Film thickness dependence of the volumetric number density of crystal nuclei in the LLDPE thin films. A volume was obtained by multiplying the observed film area by a corresponding film thickness. Here, the films thinner than 70 nm at 115 °C and the 21 nm thick film at 90 °C were annealed for 10 h (smaller symbols), and the others were annealed for 2 h. For films thinner than 150 nm, the density of crystal nuclei increases with decrease of film thickness. AFM images were used in counting the number of nuclei for the 21 and 42 nm thick films at 90 °C and OM for the other film thicknesses.

an insufficiency in the extent of lamellar branching for a complete banded spherulite. However, the morphology is filled with curved lamellar bundles, and periodic undulation in height along the bundles is observed inside the bundles. These abundant curved bundles with the periodic undulation distinguish morphology 4 from morphology 3.

While Figure 6 indicates a change in morphology with film thickness at a given crystallization temperature, it also indicates that a morphology transition occurs with crystallization temperatures at a constant film thickness. Such a transition was studied in detail for a 136 nm thick film annealed over a range of temperatures from 90 to 119 °C. The changes in morphology occur over a narrow temperature range of 110−115 °C (see Supporting Information Figure S1), with the banded spherulite morphology occurring below 110 °C and the sheaflike morphology above 115 °C. On the other hand, at 119 °C, films thinner than 200 nm exhibit the sheaflike morphology, and films thicker than 200 nm exhibit morphology 3 instead of the banded spherulite morphology.

The morphologies observed in these LLDPE films are more generally categorized with two criteria: symmetry and continuity. The symmetry in the spherulite scale can be observed in the banded spherulites and the sheaflike morphology. There is no change in morphology with rotations of any magnitudes in the banded spherulites, i.e., an infinite-fold rotation symmetry (C_∞).

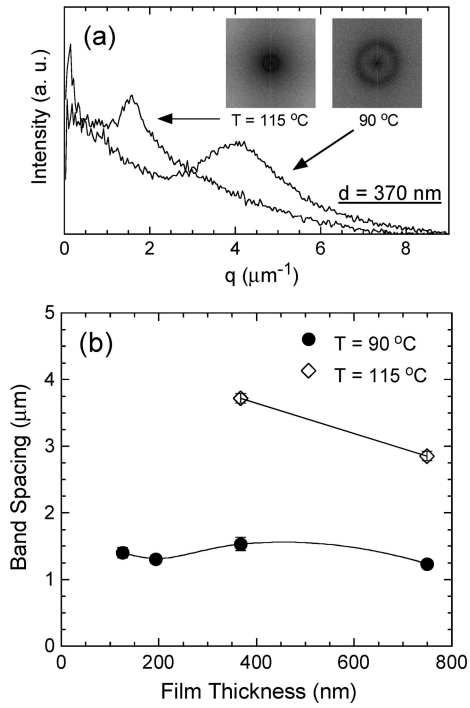

Figure 9. (a) 2D fast Fourier transformation (FFT) images of the topographic scans for the 370 nm thick films at 90 and 115 °C and the corresponding 1D power spectra obtained from the radial averaging of the 2D FFT spectra with q defined as 2π/periodicity (μm^{-1}). The original contact mode AFM images are shown in Figure 4. Average band spacing was determined from the peak positions in the 1D power spectra. (b) Average band spacing as a function of film thickness for the LLDPE thin films at 90 and 115 °C. The band spacing values of the films at 115 °C are higher than those at 90 °C.

In the sheaflike morphology, an identical morphology can be obtained by a rotation of 180°, i.e., a 2-fold rotation symmetry (C_2). No explicit symmetry occurs for the intermediate morphologies 3 and 4 with rotation. A second criterion, continuity, is applied to distinguish between the four morphologies. While morphology 3 shows frequent branching of lamellar bundles and fusing with neighboring bundles (much like the sheaflike morphology), in the case of morphology 4 the lamellar bundles are significantly less frequently branched and not fused. As summarized in Table 1, the banded spherulite morphology occurs with symmetry (C_∞) and no continuity, the sheaflike morphology with symmetry (C_2) and continuity, the morphology 3 with neither symmetry nor continuity, and the morphology 4 with continuity but no symmetry.

The morphological features observed in these LLDPE films were quantitatively analyzed in terms of fraction of edge-on lamellae, nuclei number density, and band spacing. The fraction of edge-on lamellae in these films was obtained using the threshold and histogram methods in Photoshop software and the results presented in Figure 7. For the case of the thick films (i.e., 370 and 750 nm thick films) forming banded spherulites, the fraction of edge-on lamellae is comparable at both crystallization temperatures (i.e., 90 and 115 °C). On the other hand, with decreasing film thickness this fraction of edge-on lamellae decreases: at 90 °C the most rapid changes occur in the thickness range corresponding to the intermediate morphology 4, while for the films crystallized at 115 °C the most significant changes occur over a thickness range corresponding to the transition from the intermediate morphology 3 to the sheaflike morphology.

The numbers of crystal nuclei in the isothermally crystallized thin films at 90 and 115 °C were counted in the AFM images or optical microscopy images (monitored film area: 490 × 360 μm^2) for multiple spots and multiple samples (at least 20 such spots or samples) and averaged. Figure 8 shows the volumetric number densities of nuclei obtained from the surface based areal density normalized by the film thicknesses. The number densities of crystal nuclei at comparable film thicknesses are higher for the series of samples crystallized at 90 °C compared to those at 115 °C. While this volume based nuclei number density become independent of film thickness for the thicker samples, the values sharply increase with decreasing film thickness below 150 nm at both temperatures. These observations suggest that the etched silicon substrate might provide additional heterogeneous nucleation sites for the crystallization of LLDPE.[8]

The banded structure is a result of lamellar twisting or periodic lamellar branching, and the decreasing band spacing with decreasing temperature has been previously observed in thick polyethylene films.[13,19] In order to obtain values for the average band spacing, fast Fourier transforms (FFT) were carried out using the Image Processing Tool Kit for Adobe Photoshop. Figure 9a shows the 2D FFT images for the 370 nm films crystallized at 90 and 115 °C and the corresponding 1D power spectra obtained from the radial averaging of the 2D FFT power spectra. The average band spacing values were determined from the position of the peak in the 1 D power spectra, and the results as a function of film thickness are presented in Figure 9b. The values of the films crystallized at 115 °C are larger than those obtained for the films crystallized at 90 °C, consistent with previous reports.[13,19] While the values in the films at 90 °C are ~1.5 μm and independent of film thickness, the limited data presented at 115 °C indicate a wider band spacing in the thinner film. On the other hand, the sheaflike lamellar aggregates in the 126 nm film crystallized at 115 °C show an undulation in height (Figure 4a). The periodicity of undulation is 4.0 ± 0.5 μm, which is similar to the band spacing of the 370 nm thick film at the same temperature.

Janimak et al., using a method for etching the spherulites with permanganate solutions, have previously observed a decrease in the band spacing with distance from the center of spherulite in polyethylene.[20] We investigate systematic changes with radial distance from the spherulite center in the band spacing and the amplitude of undulations in these LLDPE films using line scan profiles of contact mode AFM images. A typical line scan profile is presented in Figure 10a. The distances between consecutive peaks, and the differences in height between adjacent peak and valley were averaged over a 5 μm line scan, and these measures were taken to represent the band spacing and the amplitude, respectively. The variations as a function of distance from the spherulite center for the films crystallized at 90 and 115 °C are presented in parts b and c of Figure 10, respectively. The films crystallized at 90 °C exhibit a decrease in band spacing and amplitude as distance from the spherulite center increases. In contrast, the films at 115 °C do not show significant variations in band spacing and amplitude as a function of distance from spherulite center (Figure 10c).

The variations in band spacing and amplitude can be reconciled on the basis of the detailed molecular structure of the polymer and the relative rates of crystallization at the two temperatures of interest. The LLDPE chains in this study include small amount of short chain branches, SCBs (from 1-hexene comonomers), in the backbone with heterogeneous intermolecular distribution: the shorter chains with the more SCBs,[21] and these shorter chains act as impurities in crystallization process. It is known that the impurities such as comparatively short chains or branched chains are excluded from crystal lattice and piled up in the growing front as well as between lamellae.[22,23] The accumulated impurities cause unstable sites (or defects) on lamellar surfaces where lamellae are branched.[22] Therefore, as spherulites grow, the composition of the impurities increases, resulting in more frequent lamellar branching, thus

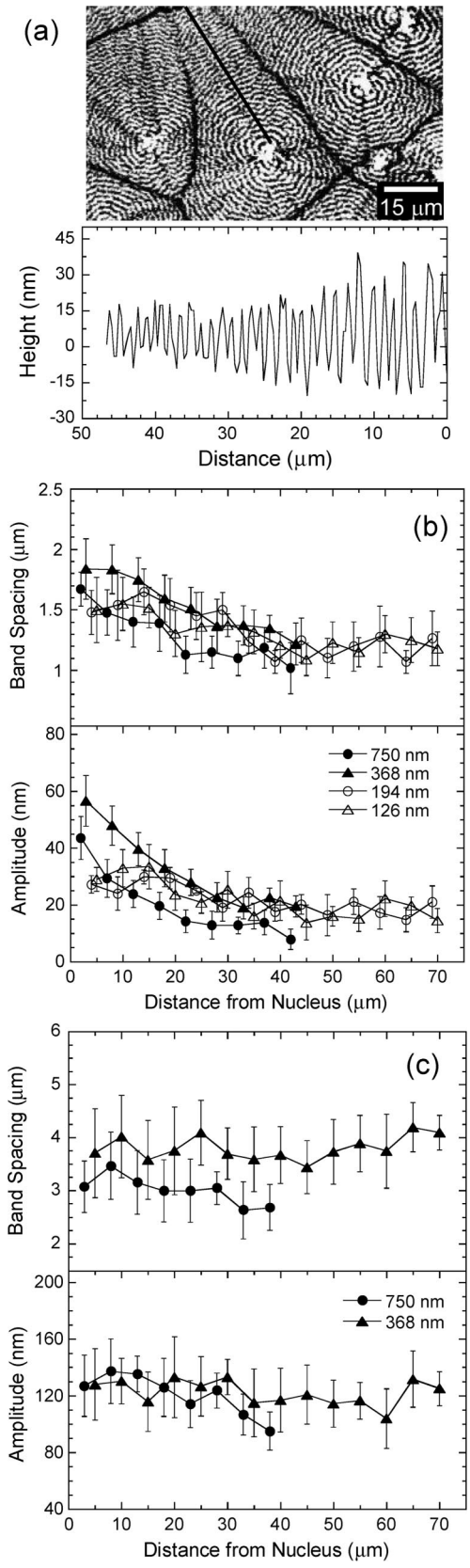

Figure 10. Dependence of the band spacing and amplitude of the bands as a function of distance from the nucleus obtained from line scan profiles of contact mode AFM images. (a) Contact mode AFM image of the 370 nm thick film at 90 °C and a typical line scan profile from the line in the image. Band spacing and amplitude as a function of distance from nucleus at (b) 90 and (c) 115 °C. The values were averaged over a 5 μm line scan, representing each range. The band spacing and amplitude decrease as the distance from the nucleus increases in the films crystallized at 90 °C.

the narrower band spacing. In the aspect of lamellar twisting, it was postulated that the segregation of impurities from the crystal region enhances the congestion at fold surfaces, giving rise to the increased bending moment. Therefore, lamellar twisting is more frequent and band spacing becomes narrower. A similar effect was observed in the linear PE fraction and its blend with polyisobutylene.[13] As for the amplitude variation, given that the variation is related to the transition of lamellar morphology between edge-on and flat-on during lamellar twisting, the large amplitude near nucleus could be due to a wider lamellar width.[19] At the higher crystallization temperature, the rate of crystallization becomes slower and the impurities are more easily dissipated in the front and sides, resulting in less effect of segregated impurities on lamellar branching and consequently band spacing.

In order to further understand the correlation between the supermolecular and lamellar morphologies and to gain insight into the lamellar structure, we undertook tapping mode AFM on films representative of the four morphologies (Figure 11). Phase angle images obtained from the tapping mode AFM imaging are able to discriminate between morphological components based on their hardness.[12,24] For the banded spherulite morphology, the thicker films exhibit edge-on lamellae, while for the thinner films a combination of edge-on and flat-on lamellae are observed. Topologically, the elevated portions correspond to edge-on lamellae in these banded morphologies. In the intermediate morphology 4 (72 nm thick film crystallized at 90 °C), the curved lamellar bundles consist of the repeated edge-on and flat-on lamellae as in the banded structure, and the lower regions (darker regions in the height image) between the lamellar bundles consist of flat-on lamellae. In Figure 11b, the intermediate morphology 3 (194 nm thick film crystallized at 115 °C) is composed of a mixture of edge-on lamellae and large flat-on lamellae. The growing directions of edge-on lamellae in different sections are less regular than in the banded spherulite, possibly due to a reduced lamellar density and less interaction between lamellae. The 72 nm thick film crystallized at 115 °C demonstrates the lamellar structures in the sheaflike morphology: the dominance of flat-on lamellae and the rare edge-on lamellar aggregates.

On the other hand, the 72 nm thick films at both temperatures show a fingerlike branched structure associated with the flat-on lamellae. While the structure can also be observed in the thinnest films (21 nm) at both temperatures (Figure 4), the fingers in the 21 nm thick film at 90 °C shows a higher aspect ratio (i.e., length/width) than at 115 °C. On the other hand, for the thicker films including the 126 nm thick film no such fingerlike structure is observed. We note that the fingerlike branched morphology has been observed previously in thin films of various polymers[25,26] and thought to occur by a diffusion-limited aggregation process (DLA).[25] In the hypothesized DLA process, the diffusing particles irreversibly stick to the closer surface of a growing aggregate, creating protruded fingers. On the basis of the observations described above for the thinnest LLDPE films, it can be surmised that the DLA process is effective at least for the ultrathin films. It is our conjecture that the DLA process occurring in such ultrathin films, representing a quasi two-dimensional system, is primarily due to the lack of sufficient supply of polymer chains. We quantify the geometrical aspects of the fingers in these films[25] with the length (measured along the growing direction of the fingers) and width (measured normal to the growth direction of the fingers). For the 21 nm film the length and width at 90 °C are 0.49 $\pm$ 0.11 and 0.11 $\pm$ 0.03 μm, respectively, while at 115 °C the corresponding values are 2.7 $\pm$ 0.7 and 1.2 $\pm$ 0.3 μm, respectively.

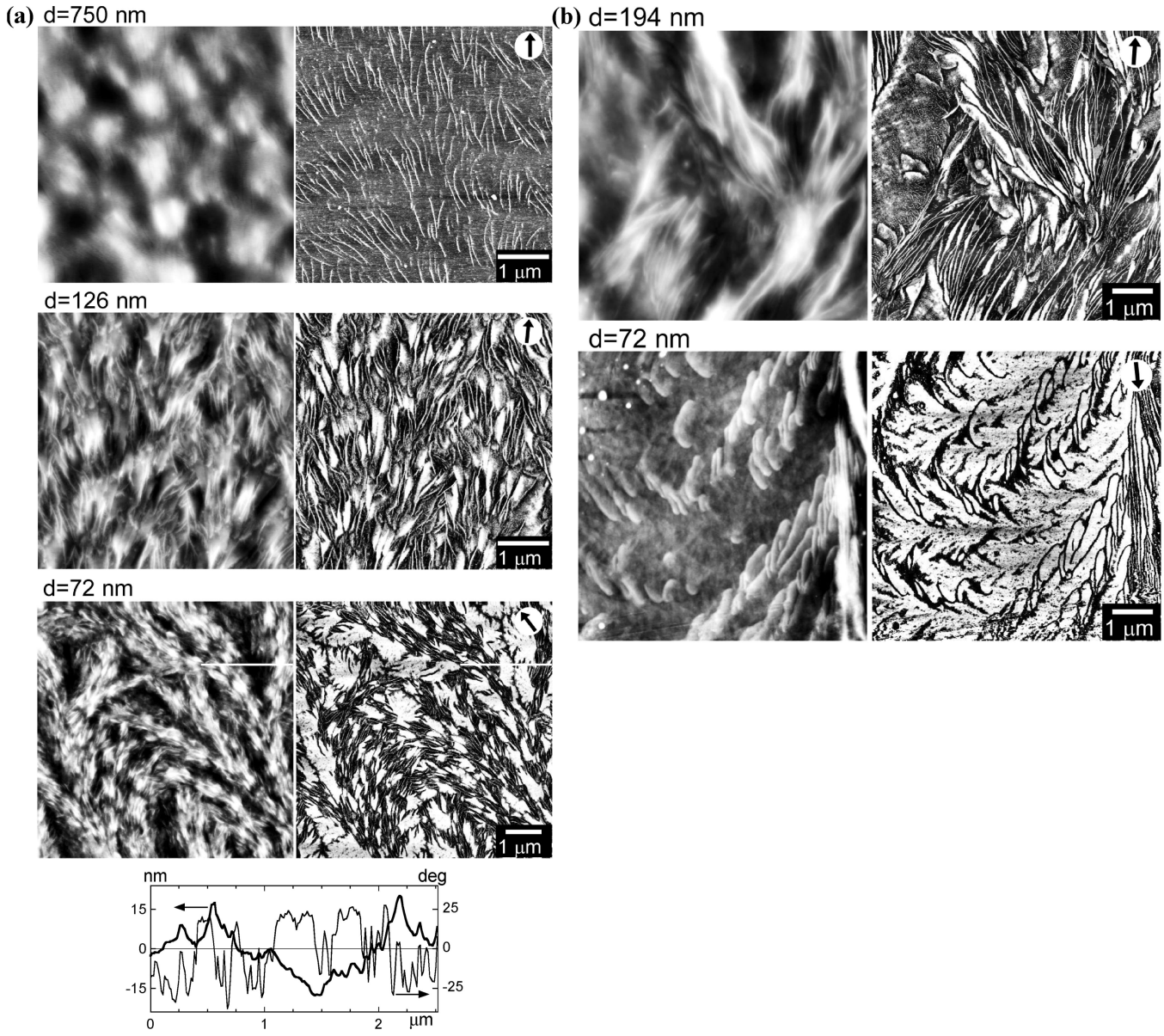

Figure 11. Tapping mode AFM images of the LLDPE thin films at (a) 90 and (b) 115 °C: height (left) and phase (right) images. The images show the detailed lamellar morphology in four different morphologies. The line scan profiles in (a) (thicker line for height profile and thinner line for phase angle profile) demonstrate that the flat-on lamellae are located in the lower region between the curved lamellar aggregates. The arrows in the phase images indicate the radial growth direction.

The occurrence of DLA processes in the ultrathin films along with the changes in the lamellar branching and the associated morphological transitions in such films might be related to the slowing down of the crystal growth rates in such films and previously implicated.[27] While a detailed investigation of the film thickness dependence of the lamellar growth rate is beyond the scope of this study, the depressed growth rate in the thinner films can be inferred by comparing the time dependence of the growth rate in the 21 nm thick film at 115 °C and the 126 nm thick film at 119 °C. The contour lengths from nucleus to end of mature lamellar aggregates in each crystal were measured and averaged for more than 30 different crystals in each film and presented in Figure 12 (also see Supporting Information). These statistics suggest that the approximate crystallization half-times ($t_{1/2}$) for the 126 nm (119 °C) and 21 nm (115 °C) thick films are 3 and 12 h, respectively. The $t_{1/2}$ values are significantly higher than those of bulk LLDPE by DSC (e.g., 0.8 min at 115 °C) as shown in Figure 1b, indicating the tremendously retarded crystallization in the films compared with the bulk. In Figure 12, we note that the contour length of the 21 nm thick film crystallized at 115 °C for 2 h is comparable to the contour length for the 126 nm thick film crystallized at 119 °C for 2 h. Comparing the growth rates, the 126 nm thick film crystallized at 119 °C shows a linear growth with time and empirically fitted to $L_c = 0.25t - 0.24$, where L_c is the contour length in micrometers and t the time in minutes. On the other hand, for the 21 nm film crystallized at 115 °C the growth is nonlinear ($L_c = 5.3t^{0.42}$ provides the best fit).[10] This nonlinear growth can be understood in the context of diffusion-limited growth as observed in polymer blends.[28] In the case of the ultrathin films the interaction between the polymer melt and the surface along with the limited supply of polymer (due to the thickness of the polymer films) results in a diffusion-limited growth. In the extremely confined environments of ultrathin films, the supply of crystallizable sequences is also very limited, and the crystallizable sequences will be more easily depleted in the growth front as crystals grow. As a result, the limited supply of crystallizable sequences combined with the diffusing away

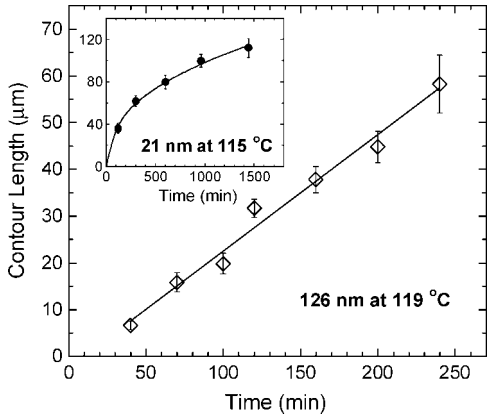

Figure 12. Contour length from center to end for mature lamellar aggregates as a function of time for the 126 nm thick films crystallized at 119 °C and the 21 nm thick films at 115 °C in the inset. The 126 nm film shows linear growth characteristics. The contour length of the 21 nm film is comparable to that of the thicker film for the annealing time of 2 h, but the growth rate of the 21 nm film is nonlinear and slowing down considerably after 2 h. These results indicate a faster growth rate for the thicker (126 nm) film, taking account of the difference, 4 °C, in crystallization temperature.

of shorter chains would induce the nonlinear growth in the 21 nm film.

The slower crystallization rate in the ultrathin films can be attributed to reduced chain mobility due to the attractive interaction between PE chains and the silicon substrate or a result of transport limitation due to confinement and the resulting two-dimensional transport of the chains or due to an altered equilibrium melting temperature of ultrathin polymers.[9] Increases in the glass transition temperature and decreases in chain diffusion rate were observed with decreasing film thickness in the polymer films with film thickness below about 150 nm on the attractive substrates.[4,29] The reduced mobility was explained by trapping or pinning of polymer chains on the attractive substrates for comparatively long periods and by chain entanglement as a medium for the long-range interaction.[30] On the other hand, Wang et al. have suggested[9] that the decreasing equilibrium melting temperature ($T_m°$) could also cause the reduced growth rate in the ultrathin films.

Concluding Remarks

The thin and ultrathin LLDPE films (20−800 nm thick) under isothermal crystallization conditions (90−119 °C) exhibited four distinct supermolecular morphologies: banded spherulite, sheaflike, and two intermediate morphologies. While these morphological transitions are restricted to the ultrathin films, there is a significant dependence on the location of these transitions with crystallization temperature and to a large extent appears to be dictated by the accommodation of defects in the polymer structure and the rate at which crystallization proceeds. It would certainly be interesting to challenge some of these notions with model linear polyethylenes or model branched polyethylenes (such as ethylene−butane copolymers), wherein the chain architecture can be carefully tailored and characterized. It is also clear that there is a significant need to understand the rate of crystallization in these ultrathin films, not only because of its consequences on the morphological development but also to understand the fundamental factors controlling the kinetics of crystallization in such thin and ultrathin films—the nature of the surface−polymer interactions, the role of confinement-induced growth limitations, and the parameters controlling bulk crystallization. Clearly, working with different surfaces such as a gold surface or alkane decorated surface might prove to be extremely useful in understanding the nature of the interactions and the extent to which it controls the rate and the supermolecular morphology.

Acknowledgment. Partial financial support from the Welch Foundation (82132), the National Science Foundation (DMR 9875321), and the Air Force Office for Scientific Research (FA9550-06-1-0422) is gratefully acknowledged.

Supporting Information Available: Figures S1 and S2. This material is available free of charge via the Internet at http://pubs.acs.org.

References and Notes

(1) (a) Despotopoulou, M. M.; Frank, C. W.; Miller, R. D.; Rabolt, J. F. *Macromolecules* **1995**, *28*, 6687. (b) Despotopoulou, M. M.; Frank, C. W.; Miller, R. D.; Rabolt, J. F. *Macromolecules* **1996**, *29*, 5797–5804. (c) Despotopoulou, M. M.; Miller, R. D.; Rabolt, J. F.; Frank, C. W. *J. Polym. Sci., Part B: Polym. Phys.* **1996**, *34*, 2335–2349. (d) Frank, C. W.; Rao, V.; Despotopoulou, M. M.; Pease, R. F. W.; Hinsberg, W. D.; Miller, R. D.; Rabolt, J. F. *Science* **1996**, *273*, 912.
(2) (a) Chatterjee, T.; Yurekli, K.; Hadjiev, V. G.; Krishnamoorti, R. *Adv. Funct. Mater.* **2005**, *15*, 1832–1838. (b) Mitchell, C. A.; Krishnamoorti, R. *Macromolecules* **2007**, *40*, 1538–1545. (c) Chatterjee, T.; Krishnamoorti, R. *Phys. Rev. E* **2007**, *75*, 050403. (d) Chatterjee, T.; Mitchell, C. A.; Hadjiev, V. G.; Krishnamoorti, R. *Adv. Mater.* **2007**, *19*, 3850. (e) Lincoln, D. M.; Vaia, R. A.; Krishnamoorti, R. *Macromolecules* **2004**, *37*, 4554–4561.
(3) Schönherr, H.; Frank, C. W. *Macromolecules* **2003**, *36*, 1188–1198.
(4) Schönherr, H.; Frank, C. W. *Macromolecules* **2003**, *36*, 1199–1208.
(5) (a) Sawamura, S.; Miyaji, H.; Izumi, K.; Sutton, S. J.; Miyamoto, Y. *J. Phys. Soc. Jpn.* **1998**, *67*, 3338–3341. (b) Beers, K. L.; Douglas, J. F.; Amis, E. J.; Karim, A. *Langmuir* **2003**, *19*, 3935–3940.
(6) Mellbring, O.; Oiseth, S. K.; Krozer, A.; Lausmaa, J.; Hjertberg, T. *Macromolecules* **2001**, *34*, 7496.
(7) Bartczak, Z.; Argon, A. S.; Cohen, R. E.; Kowalewski, T. *Polymer* **1999**, *40*, 2367.
(8) Wang, Y.; Ge, S.; Rafailovich, M.; Sokolov, J.; Zou, Y.; Ade, H.; Luning, J.; Lustiger, A.; Maron, G. *Macromolecules* **2004**, *37*, 3319–3327.
(9) Wang, Y.; Rafailovich, M.; Sokolov, J.; Gersappe, D.; Araki, T.; Zou, Y.; Kilcoyne, A. D. L.; Ade, H.; Marom, G.; Lustiger, A. *Phys. Rev. Lett.* **2006**, *96*, 028303.
(10) Godovsky, Y. K.; Magonov, S. N. *Polym. Sci., Ser. A* **2001**, *43*, 647–657.
(11) Okorn-Schmidt, H. F. *IBM J. Res. Dev.* **1999**, *43*, 351–365.
(12) Magonov, S. N.; Elings, V.; Whangbo, M.-H. *Surf. Sci.* **1997**, *375*, L385–L391.
(13) Keith, H. D.; Padden, F. J., Jr. *Macromolecules* **1996**, *29*, 7776.
(14) (a) Hoffman, J. D.; Miller, R. D. *Polymer* **1997**, *38*, 3151. (b) Armistead, J. P.; Hoffman, J. D. *Macromolecules* **2002**, *35*, 3895–3913.
(15) Keith, H. D.; Padden, F. J. *Polymer* **1984**, *25*, 28–42.
(16) (a) Bassett, D. C.; Olley, R. H.; Al Raheil, I. A. M. *Polymer* **1988**, *29*, 1539–43. (b) Bassett, D. C. *Self-Order and Form in Polymeric Materials*; Chapman & Hall: New York, 1994; p 27. (c) Toda, A.; Arita, T.; Hikosaka, M. *Polymer* **2001**, *42*, 2223–2233.
(17) Vaughan, A. S.; Bassett, D. C. *Comprehensive Polymer Science*; Pergamon Press: New York, 1989; Vol. *2*, p 415.
(18) Eppe, R.; Fisher, E. W.; Stuart, H. A. *J. Polym. Sci.* **1959**, *34*, 721.
(19) Sasaki, S.; Sakaki, Y.; Takahara, A.; Kajiyama, T. *Polymer* **2002**, *43*, 3441–3446.
(20) Janimak, J. J.; Markey, L.; Stevens, G. C. *Polymer* **2001**, *42*, 4675–4685.
(21) (a) Schouterden, P.; Groeninckx, G.; Vanderheijden, B.; Jansen, F. *Polymer* **1987**, *28*, 2099–2104. (b) Mirabella, F. M.; Ford, E. A. *J. Polym. Sci., Part B: Polym. Phys.* **1987**, *25*, 777–790. (c) Wignall, G. D.; Alamo, R. G.; Londono, J. D.; Mandelkern, L.; Stehling, F. C. *Macromolecules* **1996**, *29*, 5332–5335. (d) Wignall, G. D.; Alamo, R. G.; Ritchson, E. J.; Mandelkern, L.; Schwahn, D. *Macromolecules* **2001**, *34*, 8160–8165.
(22) (a) Keith, H. D.; Padden, F. J., Jr. *J. Appl. Phys.* **1963**, *34*, 2409. (b) Keith, H. D.; Padden, F. J., Jr. *J. Appl. Phys.* **1964**, *35*, 1270.
(23) (a) Abo el Maaty, M. I.; Bassett, D. C. *Polymer* **2000**, *41*, 9169. (b) Abo el Maaty, M. I.; Bassett, D. C.; Olley, R. H.; Jaaskelainen, P. *Macromolecules* **1998**, *31*, 7800. (c) Abo el Maaty, M. I.; Hosier, I. L.; Bassett, D. C. *Macromolecules* **1998**, *31*, 153–157.

(24) Bar, G.; Thomann, Y.; Brandsch, R.; Cantow, H.-J. *Langmuir* **1997**, *13*, 3807.
(25) Reiter, G.; Sommer, J.-U. *J. Chem. Phys.* **2000**, *112*, 4376.
(26) (a) Liang, G. D.; Xu, J. T.; Fan, Z. Q.; Mai, S. M.; Ryan, A. J. *Langmuir* **2007**, *23*, 3673–3679. (b) Koneripalli, N.; Bates, F. S.; Fredrickson, G. H. *Phys. Rev. Lett.* **1998**, *81*, 1861–1864. (c) Wang, M. T.; Braun, H. G.; Meyer, E. *Macromolecules* **2004**, *37*, 437–445.
(27) (a) Jiang, Y.; Yan, D.-D.; Gao, X.; Han, C. C.; Jin, X.-G.; Li, L.; Wang, Y.; Chan, C.-M. *Macromolecules* **2003**, *36*, 3652–3655. (b) Hu, W.; Cai, T. *Macromolecules* **2008**, *41*, 2049.
(28) (a) Wu, L.; Lisowski, M.; Talibuddin, S.; Runt, J. *Macromolecules* **1999**, *32*, 1576. (b) Okada, T.; Saito, H.; Inoue, T. *Polymer* **1994**, *35*, 5699. (c) Lee, C. H. *Polymer* **1998**, *39*, 5197.
(29) (a) Fryer, D. S.; Nealey, P. F.; de Pablo, J. J. *Macromolecules* **2000**, *33*, 6439–6447. (b) Wallace, W. E.; van Zantan, J. H.; Wu, W. L. *Phys. Rev. E* **1995**, *52*, R3329.
(30) Zeng, X. *Phys. Rev. Lett.* **1997**, *79*, 241.

MA800652P